Submitted to
31st International Conference on High Energy Physics, ICHEP02, July 24, 2002, Amsterdam
Abstract: **988**
Parallel Session **6**
www-h1.desy.de/h1/www/publications/conf/conf_list.html

Measurement of Dijet Cross-Sections with Leading Neutrons in ep interactions at HERA

H1 Collaboration

Abstract

Measurements are presented of the production in ep interactions at HERA of dijets in conjunction with a leading neutron. The energy of the neutron is required to be greater than 400 GeV and its angle with respect to the incoming proton direction less than 0.8 mrad. Differential cross-sections have been measured in the photoproduction ($Q^2 < 10^{-2}\mathrm{GeV}^2$) and deep inelastic ($2 < Q^2 < 80\ \mathrm{GeV}^2$) regimes. Monte Carlo simulations based on standard ep interaction processes or on the one-pion-exchange model and using several parameterizations for the pion structure function are compared to the measurements. Properties of the hadronic final state are further investigated by measuring, for the fraction of dijet events containing a leading neutron in the final state, the dependence on jet and kinematical variables.

1 Introduction

The cloud of virtual pions contained in the proton plays an important role in the structure of the nucleon. It has been shown (e.g. in [1, 2, 3]) that the pion-pole contribution to Deep Inelastic Scattering (DIS) can be reliably determined by studying the production of highly energetic forward neutrons. While the parton distributions of the pion in the region of Bjorken-$x \gtrsim 0.2$ have been constrained by fixed target experiments, the first measurement of pion structure at small $x (\sim 10^{-3} - 10^{-2})$ was made possible by the analysis of leading neutron data in DIS at HERA, performed by the H1 Collaboration [4]. The parton distributions of the pion can be probed in hard hadronic interactions, which are characterized by production of jets with high transverse momentum p_T. A first measurement of dijet production in events with a leading neutron in photoproduction was recently presented by the ZEUS Collaboration [5].

In this paper jet production is studied in events which contain in the final state a leading neutron n with energy $E_n > 400$ GeV and polar angle $\theta_n < 0.8$ mrad [1]. The measurements are made in the quasi-real photoproduction ($Q^2 < 10^{-2}$ GeV^2) and DIS ($2 < Q^2 < 80$ GeV^2) regimes. The cross-sections are measured differentially in Q^2, jet transverse energy E_T^{jet} and pseudorapidity η^{jet}, and in the momentum fractions of the photon and the pion carried by the interacting partons, x_γ^{jet} and x_π^{jet}. Several predictions in the form of Monte Carlo simulations are compared to the measurements.

In addition, the factorization properties of leading neutron production are studied by comparing the jet production rate in inclusive and leading neutron data samples.

2 Event selection

The data used in this analysis were collected with the H1 detector in the years 1996–97, corresponding to an integrated luminosity of $19.2\ \mathrm{pb}^{-1}$.

In the photoproduction analysis, the final state electron is detected in the electron detector of the luminosity system, which has an acceptance such that $Q^2 < 10^{-2}$ GeV^2. The scaled photon energy $y \equiv 1 - E'_e/E_e$ is required to be within $0.3 < y < 0.65$, where E'_e is the energy of the scattered electron in the electron detector and E_e is the electron beam energy (27.5 GeV).

The final state electrons in DIS are required to have polar scattering angles $156^\mathrm{o} < \theta_\mathrm{e} < 176^\mathrm{o}$ and are identified using the backward SpaCal calorimeter in combination with a track segment reconstructed in a backward drift chamber (BDC). The energy E'_e of the electron candidate was required to be greater than 10 GeV. The inclusive kinematic variables are calculated as

$$\mathrm{Q}^2 = 4\mathrm{E_e}\mathrm{E'_e}\cos^2\frac{\theta_\mathrm{e}}{2} \qquad \mathrm{y} = 1 - \frac{\mathrm{E'_e}}{\mathrm{E_e}}\sin^2\frac{\theta_\mathrm{e}}{2}$$

This analysis is restricted to the range: $2 < Q^2 < 80$ GeV^2 and $0.1 < y < 0.7$.

[1] The H1 coordinate system has its origin at the nominal interaction point and its z axis along the incoming proton direction. Polar angles θ are measured with respect to the z direction.

All events which satisfy the selection cuts are subjected to a jet search using a cone algorithm with radius $R = \sqrt{\Delta\eta^2 + \Delta\phi^2} = 1$. The jet finding is performed in the $\gamma^* p$ center of mass frame, with transverse energies calculated relative to the γ^* axis in that frame. Exactly two jets with transverse energy $E_T^{jet} > 6$ GeV are required. To ensure that the bulk of the jet energy is restricted to the region covered by the LAr calorimeter, events are only considered if both jets lie within the region of laboratory pseudorapidity $-1 < \eta^{jet} < 2$.

Leading neutrons are detected in the Forward Neutron Calorimeter (FNC) which consists of lead and scintillator fibres and which is located 107 m away from the nominal H1 interaction point in the proton beam direction (for details see [4]). The acceptance of the FNC is defined by the aperture of the HERA beam pipe magnets and corresponds to neutron scattering angles of $\theta_n \lesssim 0.8$ mrad. For this analysis the energy of the neutron in the FNC is required to be $E_n > 400$ GeV.

The final photoproduction data sample contains about 80,000 dijet events of which 605 events satisfy the neutron identification requirement. In the DIS sample 25,000 dijet events are selected, of which 334 events contain a leading neutron.

3 Monte Carlo models

In order to correct the data distributions for biases and losses due to the apparatus, to correct for the effects of QED radiation and to compare theoretical models with the data, several Monte Carlo generator programs are used.

POMPYT [6] and RAPGAP [7] simulate leading neutron production using pion exchange. In these programs, the cross-section for leading neutron production is proportional to the product of a pion flux factor and a pion structure function. In the present analysis the pion flux factor is taken from Holtmann et al. [1]. The pion parton distributions are simulated according to the GRV-π-LO parameterizations [8]. For the comparisons with data, predictions based on other pion parton distributions are also used [9].

Standard fragmentation mechanisms which produce leading neutrons are used in the Monte Carlo event generators PYTHIA [10], DJANGO [11] and RAPGAP.

In general, the Monte Carlo simulations describe all relevant reconstructed distributions well.

4 Results

Figure 1 shows the distributions of the energy of the neutrons measured in the FNC before correction for detector inefficiencies and acceptance effects, together with the expectations from Monte Carlo simulations. Models which do not explicitly include the pion exchange mechanism (PYTHIA, RAPGAP) fail to reproduce acceptably the neutron energy spectrum, predicting distributions which are shifted towards lower energies. POMPYT and RAPGAP, on the other hand, describe the energy spectrum well for $E_n \gtrsim 400$ GeV, thereby demonstrating the necessity in the

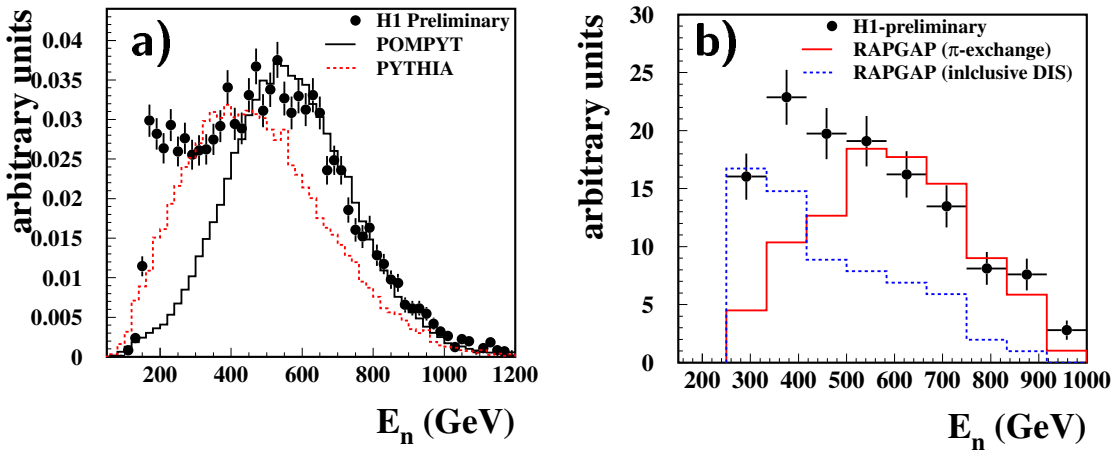

Figure 1: The distributions of leading neutron energy E_n for data and Monte Carlo detector simulations. Figure 1a and 1b correspond to the photoproduction ($Q^2 \sim 0$) and DIS ($2 < Q^2 < 80$ GeV^2) regimes, respectively.

FNC energy spectrum for a colour singlet component in the proton manifest in the form of pion exchange and its explicit contribution to leading neutron production. The large difference between data and Monte Carlo simulations at low E_n is due to the contribution of processes other than pion exchange and to background from neutral electromagnetic particles (π^0, γ), which is present in the data but not in the Monte Carlo simulations used for this analysis. For neutron energies above $E_n > 400$ GeV this contribution is below 1% and is neglected in the following. The high-energy tail of the neutron energy spectrum is due to deterioration of the FNC energy response which leads to an over-estimation of the incident particle's energy and worsening of energy resolution.

The resulting cross-sections for dijet production with $E_T^{jet} > 6$ GeV and events with $E_n > 400$ GeV and $\theta_n < 0.8$ mrad are shown in Figs. 2–3 for the photoproduction and in Fig. 4 for the DIS measurements. E_T^{jet} and η^{jet} are the jet transverse energy and pseudorapidity (positive η^{jet} corresponds to the proton direction). x_γ^{jet} and x_π^{jet} are the fractional momenta of the photon and pion carried by the partons involved in hard interaction. x_γ^{jet} and x_π^{jet} are calculated from the jet E_T^{jet} and η^{jet} as follows:

$$x_\gamma^{jet} = (E_{T,1}^{jet} e^{-\eta_1^{jet}} + E_{T,2}^{jet} e^{-\eta_2^{jet}})/2yE_e \qquad x_\pi^{jet} = (E_{T,1}^{jet} e^{\eta_1^{jet}} + E_{T,2}^{jet} e^{\eta_2^{jet}})/2(E_p - E_n)$$

Here $E_e = 27.5$ GeV and $E_p = 820$ GeV are the incident electron and proton beam energies. The ep cross-sections are corrected to the Born level using the HERACLES interface to the RAPGAP Monte Carlo program. In the figures the inner error bars represent the statistical errors, while the outer error bars show the quadratic sum of the statistical and systematic errors. The total systematic errors are about 27% for the photoproduction and about 32% for the DIS measurements. In Fig. 4 (DIS) the overall normalization error of $\sim 25\%$ is not shown.

In Figs. 2-4 the different Monte Carlo predictions are compared with the measured cross-sections. All Monte Carlo models used for comparison, also PYTHIA which does not simulate

pion exchange, provide satisfactory descriptions of the data distributions, both in shape and normalization.

In the framework of the one-pion-exchange model as implemented in POMPYT, the sensitivity of the measurement to different choices for the pion structure function [9] is presented in Fig. 3. It is clear that with the present level of experimental uncertainty, no preference for any of the pion structure function parameterizations can yet be given.

5 Test of factorization

Assuming factorization, no correlations between the hadron production in the current and target fragmentation regions are expected. Factorization is studied here by measuring the fraction of events with a leading neutron in the inclusive dijet sample as a function of the jet kinematical variables.

Results are shown in Fig. 5 as functions of jet E_T^{jet} and x_γ^{jet}. Only the photoproduction data was used for this measurement. The inner error bars represent the statistical errors, while the outer error bars are the quadratic sum of statistical and systematic errors. The systematic errors are highly correlated, since the main source of systematic errors is the uncertainty of the FNC acceptance. The events with a leading neutron with $E_n > 400\,\mathrm{GeV}$ amount to about $3-3.5\%$ of the inclusive dijet sample. The fraction of leading neutron events is almost flat in jet E_T, while it exhibits a strong dependence on x_γ^{jet}– at high x_γ^{jet} it is twice as large as at low x_γ^{jet}. Possible explanations of this rise can be kinematics of the processes, or differences either in the remnant interactions or in the parton distributions involved in leading neutron events as compared to the inclusive sample.

In order to study the transition from photoproduction to DIS the fraction of leading neutron events as a function of Q^2 was measured. The resulting distribution is shown in Fig.6. The distribution does not show significant deviations from flatness.

These observations are in general agreement with the factorization hypothesis.

6 Summary

Measurements of the differential jet cross-sections are presented as a function of E_T^{jet}, η^{jet}, x_γ^{jet} and x_π^{jet} in photoproduction ($Q^2 < 10^{-2}\mathrm{GeV}^2$) and in deep inelastic ep scattering ($2 < Q^2 < 80\ \mathrm{GeV}^2$) for events with an energetic forward neutron (leading neutron) in the final state.

Models which do not include pion exchange fail to describe the neutron energy spectrum. Models which include one pion exchange describe the neutron energy spectrum well, thereby establishing the need for a colour singlet component of proton structure which is manifest in the form of pion exchange and leading neutron production. The models also reproduce the observed jet differential production cross sections. Within the present experimental uncertainties of this measurement, it is not yet possible to discriminate between different parameterizations of the pion structure function.

The observed fraction of dijet events with a leading neutron shows no significant dependence on values of the jet E_T or on the scale Q^2, in agreement with the hypothesis that the proton-pion and pion-photon vertices are independent.

References

[1] H. Holtmann et al., *Phys.Lett*. **B338** (1994) 363.

[2] B. Kopeliovich, B. Povh and I. Potashnikova, *Z. Phys.* **C73** (1996) 125.

[3] M. Przybycień, A. Szczurek and G. Ingelman, *Z. Phys.* **C74** (1997) 509.

[4] H1 Collaboration, C. Adloff et al., *Eur. Phys.J*. **C6** (1999) 587.

[5] ZEUS Collaboration, J. Breitweg et al., *Nucl. Phys.*. **B596** (2001) 3.

[6] P.Bruni, G. Ingelman, *Proceedings of the Europhysics Conference, Marseille, France, July 1993, p.595*;
(see also http://www3.tsl.uu.se/thep/pompyt)

[7] RAPGAP, H. Jung, *Comp. Phys. Comm.* **86** (1995) 147;
(see also http://www.desy.de/~jung/rapgap.html)

[8] M. Glück, E. Reya and A. Vogt, *Z. Phys.* **C53** (1992) 651.

[9] J.F. Owens, *Phys.Rev.* **D30** (1984) 943;
P.J. Sutton et al., *Phys.Rev.* **D45** (1992) 2349.

[10] PYTHIA Version 5.722, T. Sjöstrand, *Comp. Phys. Comm.* **82** (1994) 74;
T. Sjöstrand, "PYTHIA 5.7 and JETSET 7.4", CERN-TH.7112/93 (1993) (revised Feb. 1994).

[11] DJANGO, G.A. Schuler and H. Spiesberger, Proceedings pf the Workshop *Physics at HERA,* Eds. W. Buchmüller and G. Ingelman, Vol.3 (1991) 1419.

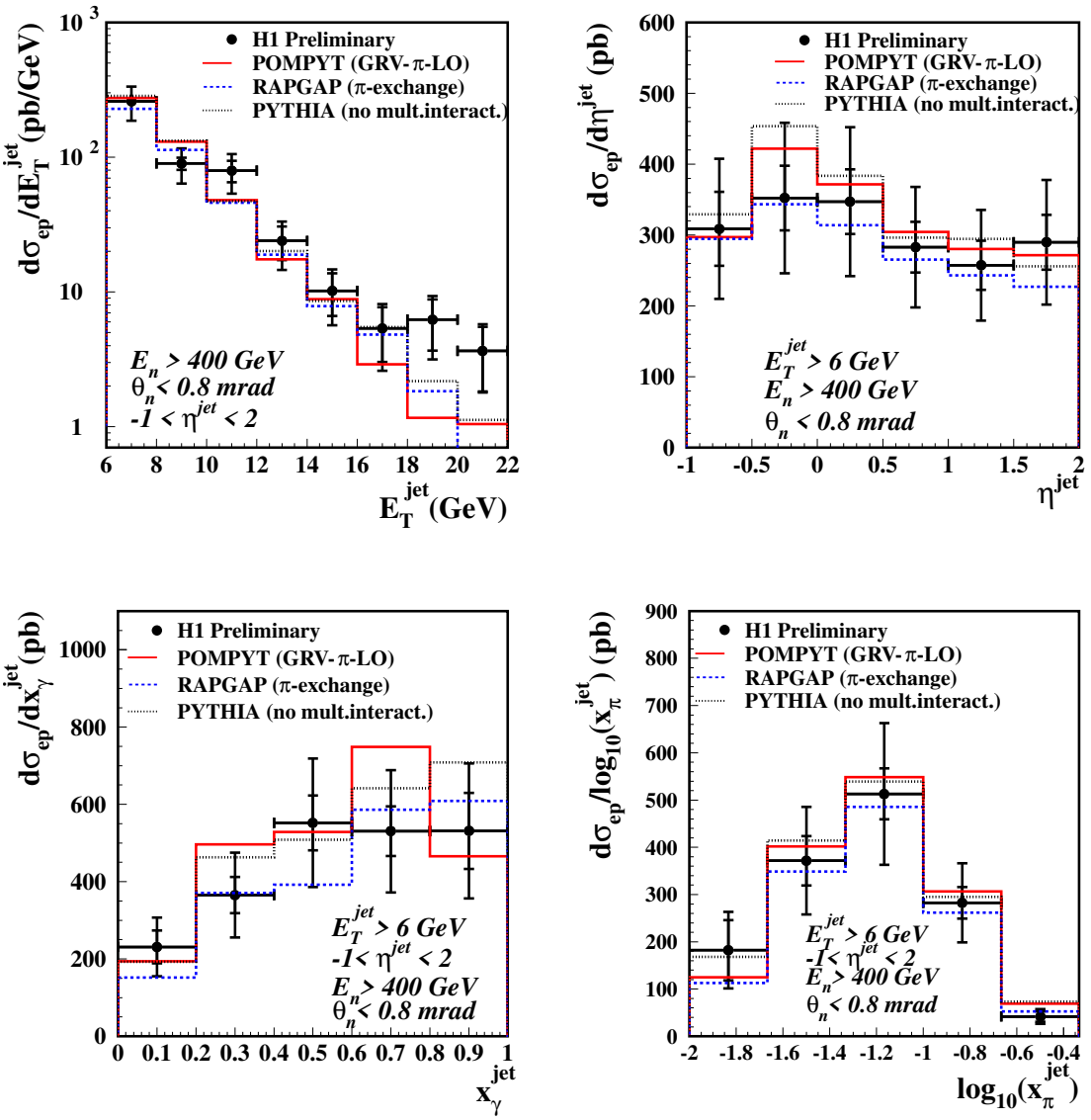

Figure 2: Dijet differential ep cross-sections as a function of jet E_T^{jet}, η^{jet}, x_γ^{jet} and x_π^{jet} for events with $E_T^{jet} > 6$ GeV, $-1 < \eta^{jet} < 2$ and with a leading neutron $E_n > 400$ GeV, $\theta_n < 0.8$ mrad. The cross-sections correspond to the kinematical range $Q^2 < 10^{-2}\text{GeV}^2$ and $0.3 < y < 0.65$. POMPYT, RAPGAP and PYTHIA Monte Carlo predictions are compared to the measurements.

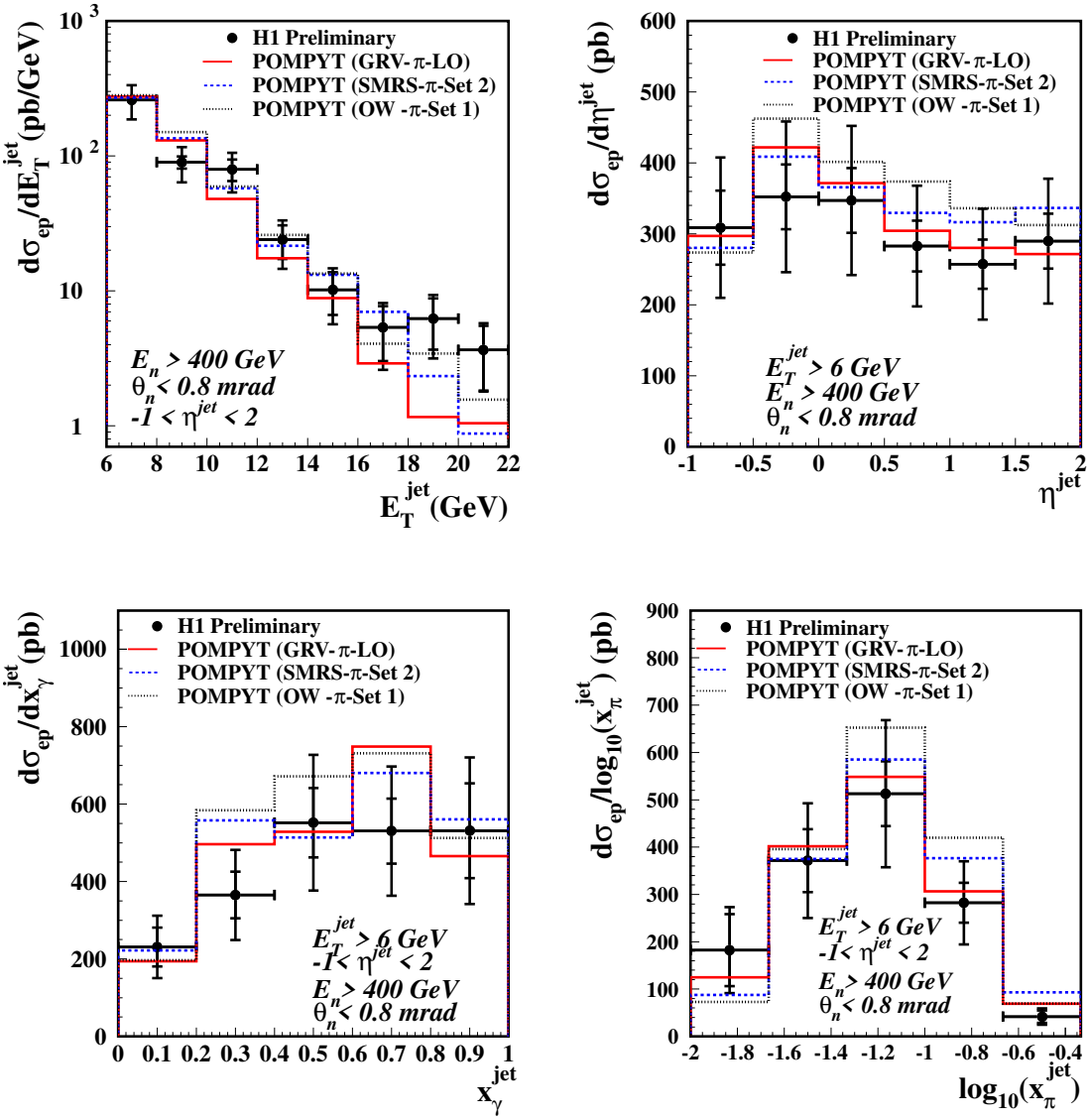

Figure 3: Dijet differential ep cross-sections as a function of jet E_T^{jet}, η^{jet}, x_γ^{jet} and x_π^{jet} for events with $E_T^{jet} > 6$ GeV, $-1 < \eta^{jet} < 2$ and with a leading neutron $E_n > 400$ GeV, $\theta_n < 0.8$ mrad. The cross-sections correspond to the kinematical range $Q^2 < 10^{-2}\text{GeV}^2$ and $0.3 < y < 0.65$. POMPYT Monte Carlo predictions using different parameterizations for the parton distributions in the pion are compared to the measurements.

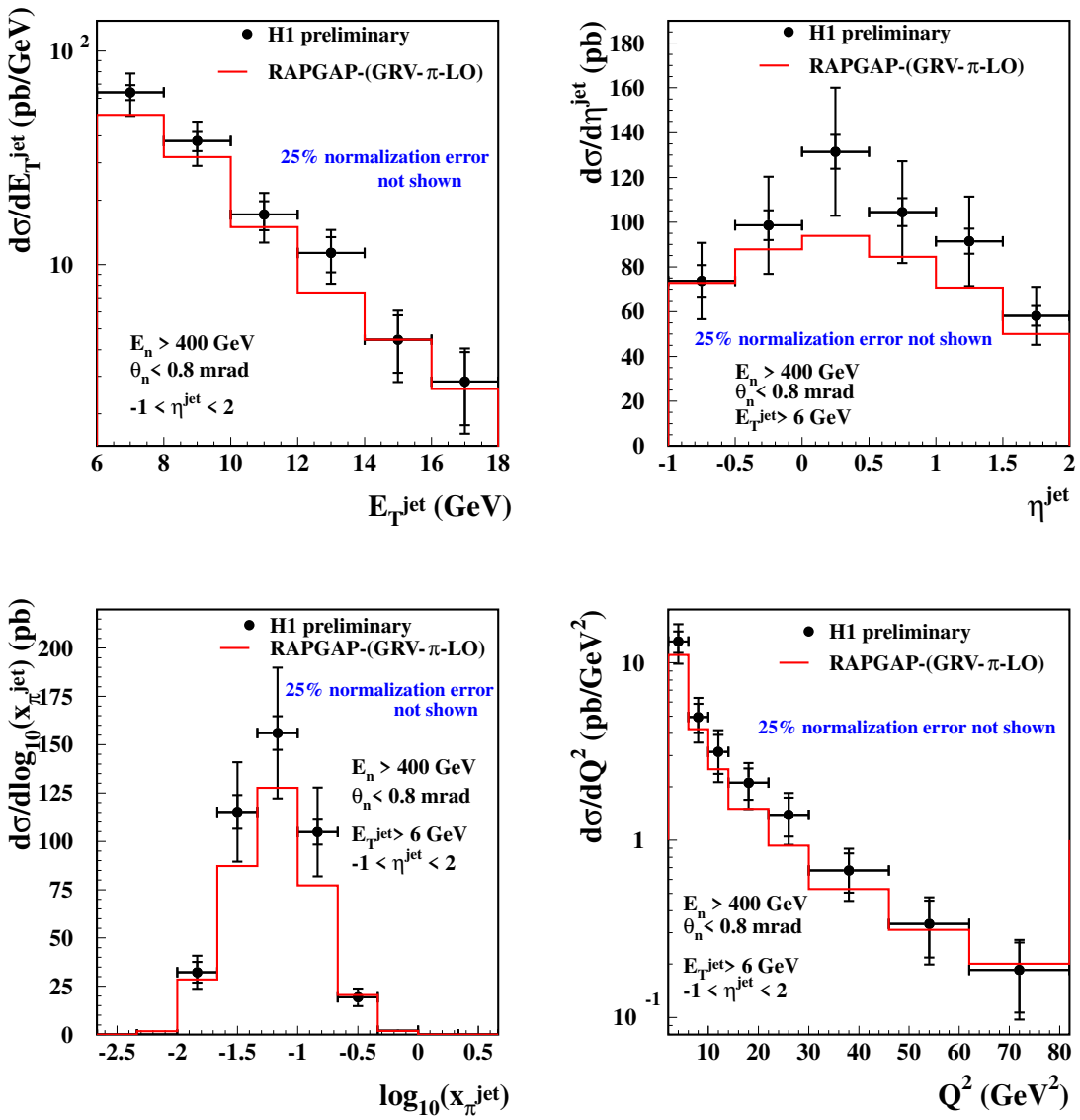

Figure 4: Dijet differential cross-sections as function of jet E_T^{jet}, η^{jet}, Q^2 and x_π^{jet} for events with $E_T^{jet} > 6$ GeV, $-1 < \eta^{jet} < 2$ and with a leading neutron $E_n > 400$ GeV, $\theta_n < 0.8$ mrad. The cross-sections correspond to the kinematical range $2 < Q^2 < 80\text{GeV}^2$. RAPGAP Monte Carlo predictions, in which pion exchange is included, are compared to the measurements.

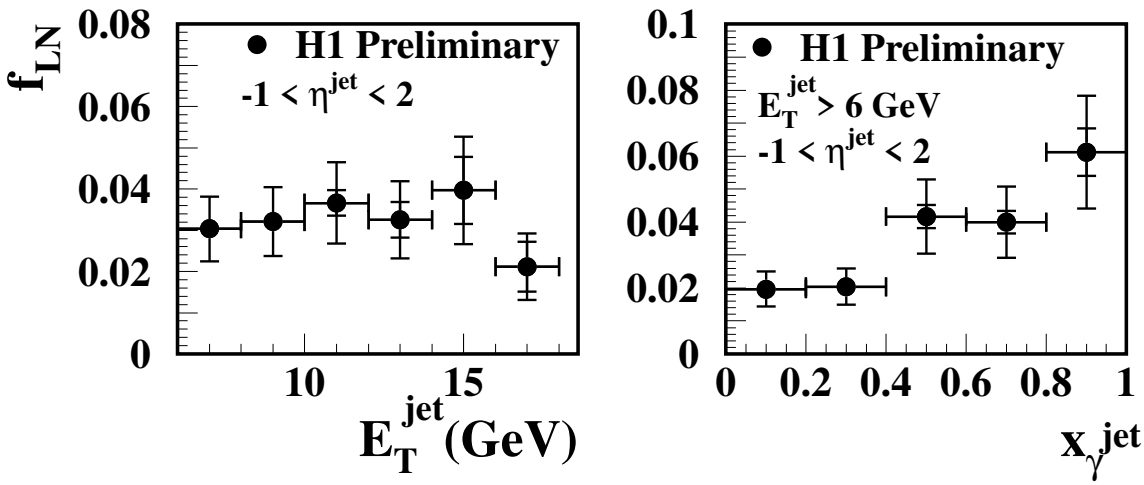

Figure 5: The fraction of dijet events with a leading neutron in photoproduction as a function of E_T^{jet} and x_γ^{jet} for events with $E_T^{jet} > 6\ GeV$, $-1 < \eta^{jet} < 2$.

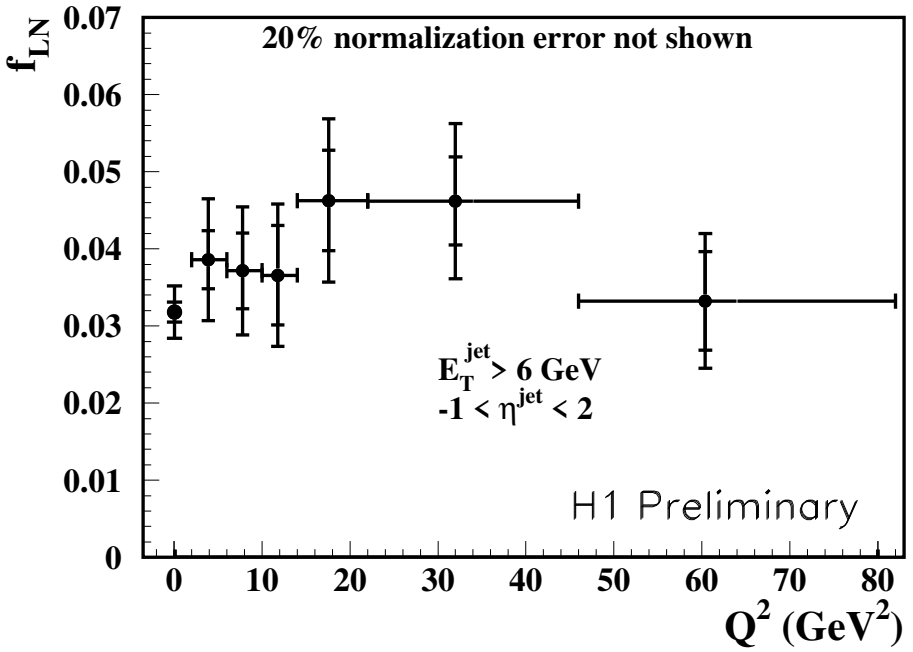

Figure 6: The fraction of dijet events with a leading neutron as a function of Q^2. The first point ($Q^2 \sim 0$) corresponds to photoproduction.